Published in final edited form as:
Biomaterials. 2013 September ; 34(28): 6695–6705. doi:10.1016/j.biomaterials.2013.05.040.

Bioelectric modulation of wound healing in a 3D *in vitro* model of tissue-engineered bone

Sarah Sundelacruz[1], **Chunmei Li**[1], **Young Jun Choi**[2], **Michael Levin**[3], and **David L. Kaplan**[1,*]

[1]Department of Biomedical Engineering, Tufts University, Medford, MA, USA

[2]Department of Chemical and Biological Engineering, Tufts University, Medford, MA, USA

[3]Department of Biology, and Center for Regenerative and Developmental Biology, Tufts University, Medford, MA, USA

Abstract

Long-standing interest in bioelectric regulation of bone fracture healing has primarily focused on exogenous stimulation of bone using applied electromagnetic fields. Endogenous electric signals, such as spatial gradients of resting potential among non-excitable cells *in vivo*, have also been shown to be important in cell proliferation, differentiation, migration, and tissue regeneration, and may therefore have as-yet unexplored therapeutic potential for regulating wound healing in bone tissue. To study this form of bioelectric regulation, there is a need for three-dimensional (3D) *in vitro* wound tissue models that can overcome limitations of current *in vivo* models. We present a 3D wound healing model in engineered bone tissue that serves as a pre-clinical experimental platform for studying electrophysiological regulation of wound healing. Using this system, we identified two electrophysiology-modulating compounds, glibenclamide and monensin, that augmented osteoblast mineralization. Of particular interest, these compounds displayed differential effects in the wound area compared to the surrounding tissue. Several hypotheses are proposed to account for these observations, including the existence of heterogeneous subpopulations of osteoblasts that respond differently to bioelectric signals, or the capacity of the wound-specific biochemical and biomechanical environment to alter cell responses to electrophysiological treatments. These data indicate that a comprehensive characterization of the cellular, biochemical, biomechanical, and bioelectrical components of *in vitro* wound models is needed to develop bioelectric strategies to control cell functions for improved bone regeneration.

*corresponding author: David L. Kaplan, 4 Colby Street, Tufts University, Medford, MA 02155 USA, 1 617 627 3251 (phone), 1 617 627 3231 (fax), David.Kaplan@tufts.edu.
Sarah Sundelacruz, 4 Colby Street, Tufts University, Medford, MA 02155 USA, 1 617 627 2670 (phone), 1 617 627 3231 (fax), Sarah.Sundelacruz@tufts.edu
Chunmei Li, 4 Colby Street, Tufts University, Medford, MA 02155 USA, 1 617 627 2580 (phone), 1 617 627 3231 (fax), chunmei.li@tufts.edu
Young Jun Choi, 4 Colby Street, Tufts University, Medford, MA 02155 USA, 1 617 627 3900 (phone), 1 617 627 3991 (fax), young.choi@tufts.edu
Michael Levin, Suite 4600, 200 Boston Avenue, Tufts University, Medford, MA 02155 USA, 1 617 627 6161 (phone), 1 617 627 6121 (fax), Michael.Levin@tufts.edu

1. Introduction

Endogenous electrical signals play an instructive role in many cellular behaviors, including *in vitro* cell proliferation, differentiation, and migration, and *in vivo* tissue wound healing and regeneration [1–5]. Endogenous wound electric fields (EFs) have been measured in a wide range of wounded and regenerating tissues, including amputated newt limbs, bone fractures, corneal wounds, and skin wounds [6–9]. In these injured tissues, a potential difference results from ion flux across leaky cell membranes or disrupted tissue barriers, establishing a wound EF. Disruption of the electrical currents that result from the wound EF has been shown to interfere with regeneration events, demonstrating that these currents are necessary for tissue regeneration [10, 11]. Application of exogenous fields can also induce a degree of regeneration in cases where regeneration does not normally occur [12–14]. On the cellular level, exogenously-applied EFs within the physiological range have been shown to act as a guidance cue for migration in numerous cell types, including keratinocytes, corneal epithelial cells, and human bone marrow mesenchymal stem cells (hMSCs), and can be adjusted to direct migration toward or away from a wound [15, 16]. Electrical signaling may also coordinate the participation of the nervous and vascular systems in the wound healing process. EFs stimulate nerve sprouting toward the wound, migration of vascular endothelial cells, and angiogenesis [17, 18]. Altogether, these observations point to a critical role for electrical signaling in wound healing, and suggest that current strategies for directed tissue repair and regeneration may benefit from a bioelectric approach.

Bone healing is often studied *in vivo* by creating an artificial fracture, then applying cells or soluble factors into the defect or implanting engineered bone constructs [19, 20]. Numerous fracture models have been developed to study different repair outcomes, including normal fracture repair, delayed union, nonunion, segmental defects, and fractures at risk of impaired healing, and have been established in a wide range of animal species, including rat, mouse, rabbit, dog, primate, sheep, pig, and cat [21]. In general, the bone repair process has been partitioned into several characteristic stages: initial inflammatory response, soft callus formation, hard callus formation, initial bony union and bone remodeling [22]. The *in vivo* environment provided by animal models successfully captures the three-dimensional (3D) nature of cell-cell and cell-matrix interactions that occur during these phases of repair, overcoming the two-dimensional (2D) limitations imposed by monolayer cell culture. However, animal fractures may not accurately reflect the biochemistry, biomechanics, anatomy, physiology, and healing processes of human fractures [21, 23]; thus, designing an animal model that adequately models human bone repair can be challenging.

To better understand bioelectric regulation of bone regeneration, there is a need for *in vitro* human tissue systems in which this form of control can be studied. Electric signaling in *in vitro* bone has been studied mostly in the context of exogenously-applied electrical stimulation of osteogenic cells in 2D and 3D cultures [24–27]. Because of the multiple cellular processes affected by applied electric fields, mechanistically integrating data on electric field effects with biochemical and genetic pathways requires an *in vitro* system in which transmembrane potential in key cells can be directly regulated by manipulation of ion conductances in the cell membrane. However, to our knowledge, there have been no studies of the role of endogenous electrical properties, as distinct from exogenously-applied stimulation, in osteoblast physiology in a 3D model. Hence, there is a need for a 3D *in vitro* model of bone wound healing as a platform in which to study human osteoblast electrophysiology during tissue repair. This approach would provide an *in vitro* mimic for *in vivo* conditions with relevant 3D features, allowing more control of the system than can be achieved *in vivo* and providing options for statistical validation. Such an *in vitro* model could provide insight into key therapeutic directions to pursue *in vivo*.

In this study, we developed a 3D tissue model of osteoblast wound healing to examine the effects of electrophysiological modulation on bone regeneration. Bone constructs were created by differentiating hMSCs into osteoblasts on porous silk fibroin scaffolds [28]. The engineered bone was cut in half to simulate wounding, and cell migration and differentiation in the wound were studied. In this wound model, osteoblast electrophysiology was modulated by adding various ion channel-targeting pharmacological agents or by changing the extracellular ionic content. The goal of this study was to demonstrate the utility of a bone wound healing model that can serve as a screening platform to identify compounds that stimulate bone differentiation and regeneration and a tractable model in which to dissect the mechanisms by which bioelectric signals regulate cellular behaviors.

2. Materials and Methods

2.1 hMSC cultivation

Whole bone marrow aspirate from a 25-year old healthy male was purchased from Lonza, and hMSCs were isolated as we have previously reported [29]. Fluorescence activated cell sorting confirmed the presence of the cell surface antigens CD105, CD73, and CD90 in the harvested hMSCs [30]. Cells were expanded in tissue culture flasks in Dulbecco's Modified Eagle Medium (DMEM) supplemented with 10% fetal bovine serum (FBS), penicillin (100 U/mL), streptomycin (100 μg/mL), 0.1 mM non-essential amino acids, and basic fibroblast growth factor (bFGF, 1 ng/mL) (Invitrogen, Carlsbad, CA). Cells were maintained in a humidified incubator at 37°C with 5 % CO_2 and 5% O_2 until initiation of differentiation. Medium was changed every 3–4 days until confluence, when cells were then trypsinized with 0.25% trypsin-1mM EDTA (Invitrogen), and frozen in liquid nitrogen in FBS with 8% DMSO.

2.2 hMSC differentiation

To stimulate bone formation, hMSC-seeded scaffolds were cultured in osteogenic (OS) medium, consisting of α-MEM supplemented with 10% FBS, penicillin (100 U/mL), streptomycin (100 μg/mL), 10 mM β-glycerophosphate, 0.05 mM L-ascorbic acid-2-phosphate, and 100 nM dexamethasone (Sigma-Aldrich, St. Louis, MO). Undifferentiated hMSCs were maintained in control medium, consisting of DMEM supplemented with 10% FBS, penicillin (100 U/mL), streptomycin (100 μg/mL), and 0.1 mM non-essential amino acids.

2.3 Electrophysiology-modulating compounds

Cells were treated with several electrophysiology-modulating compounds, which were added to osteogenic medium. These include glibenclamide (GL, 10 μM), monensin (MO, 10 nM), barium chloride (BA, 100 μM), and potassium gluconate (High K^+, HK, 40 mM) (Sigma-Aldrich).

2.4 Silk scaffold preparation

Silk fibroin was isolated from *Bombyx mori* cocoons as described previously [28]. Briefly, sericin was extracted from cocoons by boiling in 0.2 M sodium carbonate and rinsing in distilled water. The remaining silk fibroin was dissolved in 9.3 M LiBr for 4 hr at 60°C, then dialyzed for 48 hours in dia lysis cassettes with 3500MW cutoff (Pierce, Rockford, IL). Dialyzed silk solution was centrifuged twice at 9000 rpm and 4°C for 20 minutes, then diluted to a 6% so lution with distilled water. Silk solution was cast into cylindrical containers filled with NaCl granules of diameters of 500–600 μm and allowed to solidify for 72 hours. Salt crystals were leached from scaffolds by rinsing in distilled water for 48 hours to obtain porous scaffolds.

2.5 3D bone wound model

Tissue-engineered bone was generated by differentiating hMSCs on porous silk scaffolds. One million hMSCs were seeded onto each silk scaffold (6 mm diameter × 3 mm height) and were differentiated toward osteoblasts for six weeks. Silk scaffolds were wounded by cutting the tissue in half in cross-section, and inserting a fresh unseeded silk scaffold (6 mm diameter × 1.5 mm height) between the two cut halves of the tissue, simulating implantation of a silk scaffold into a bone defect [31]. The triple-layered structure was held together by a thin stainless steel wire inserted through the center of the scaffolds with two rubber stoppers at either end securing the scaffolds together. The constructs were cultured for an additional six weeks, with or without electrophysiology-modulating compounds in the medium. GL, MO, BA, and HK were added for the entire six weeks following wounding. One group was treated with HK for the first three weeks after wounding, followed by BA for the last three weeks (KB). At the end of the total twelve weeks, the scaffolds were harvested for analysis of cell ingrowth and osteogenic differentiation (Figure 1A).

2.6 Assessment of OS differentiation

Matrix calcification was determined by a colorimetric assay using the Calcium (CPC) Liquicolor Test (Stanbio Laboratory, Boerne, TX). Calcium was dissociated with trichloroacetic acid and reacted with o-cresolphthalein complexone. The colored reaction product was measured spectrophotometrically at 575 nm using a microplate reader (VersaMax, Molecular Devices, Sunnyvale, CA). Mineral deposition was also visualized by Alizarin Red staining. Samples were fixed in 10% formalin, embedded in paraffin, cut into 8 μm sections, and stained with Alizarin Red S (Sigma-Aldrich). Quantitative real time PCR was used as previously described to quantify expression of several bone markers, including runt-related transcription factor 2 (Runx2), Collagen I alpha 1 (Col 1), alkaline phosphatase (ALP), and bone sialoprotein (BSP). Briefly, total RNA was isolated from hMSCs using Trizol reagent (Invitrogen) following the single step acid-phenol guanidinium method, and purified using the Qiagen RNEasy kit (Qiagen, Valencia, CA). Reverse transcription was performed on the purified RNA using the High Capacity cDNA Reverse Transcription kit (Applied Biosystems, Foster City, CA). Transcript expression levels were quantified a Stratagene Mx3000P QPCR System (Stratagene, La Jolla, CA). Primers and probes for bone-related genes were obtained from TaqMan® Gene Expression Assay kits (Applied Biosystems). Expression levels were normalized to the housekeeping gene glyceraldehyde 3-phosphate dehydrogenase (GAPDH) and reported relative to untreated OS cells. We have previously reported PCR reaction conditions and primers [31].

2.7 Assessment of cell content

Cell content of scaffolds was assessed with the Quant-iT Picogreen dsDNA assay according to the manufacturer's instructions (Invitrogen). Additionally, cell distribution within the scaffolds was visualized by histological staining of scaffold sections. Scaffolds were fixed in 10% formalin, embedded in paraffin, cut into 8 μm sections, and stained with hemotoxylin and eosin for nuclei and cytoplasm.

2.8 Confocal imaging using voltage-sensitive fluorescent dye

OS-differentiated hMSCs were stained with a voltage-sensitive fluorescent dye [29, 32]. Bis-(1,3-diethylthiobarbituric acid)trimethine oxonol (DiSBAC, Invitrogen) is an anionic voltage-sensitive dye whose uptake into cells is voltage-dependent: higher uptake is seen in more depolarized cells. A fresh solution of 10 mM DiSBAC in DMSO was prepared and diluted to 0.5 μM in Hank's Buffered Salt Solution (HBSS, Invitrogen). Cells grown in glass-bottom dishes (poly-d-lysine coated, No. 1.5, MatTek Corp., Ashland, MA) were incubated in DiSBAC for 20 minutes at 37°C, equilibrated to room temperature for 10

minutes, then imaged while submerged in dye. Images were acquired on a Leica TCS SP2 laser scanning confocal microscope with an inverted DM IRE2 stand (Wetzlar, Germany) and a Leica PL APO 63x (NA 1.2) water-immersion objective. DiSBAC was excited with a 543 nm HeNe laser; images were collected at 570 ± 5 nm by a non-descanned PMT controlled by Leica Confocal Software. A double dichroic filter was used to eliminate excitation light. To visualize membrane potential changes, cells at resting potential were imaged as above, exposed to test compound and allowed to equilibrate for 5 min, then imaged once more. MATLAB software (The MathWorks, Inc.) was used to assist in the drawing of regions of interest (ROI) around cells and in calculating pixel intensities within the ROIs. ROIs were drawn on thresholded images by using the function bwboundaries to trace cells and their nuclei. Fluorescence intensities of cells encircled by ROIs were calculated by averaging corresponding pixel intensities in the original image, excluding pixels within encircled nuclei, after background correction using a blank (no cell) region of the image.

2.9 Statistics

Data are reported as means ± standard deviation. One-way ANOVA statistical analysis was performed, followed by the Tukey-Kramer post-hoc test. In bar graphs, means labelled with the same letter are not significantly different from one another (Tukey-Kramer, $p>0.05$).

3. Results

3.1 Membrane voltage response to pharmacological modulation

To quantify the effects of our chosen pharmacological reagents on membrane potential (V_{mem}) of osteogenic-differentiated hMSCs, we used the voltage-sensitive fluorescent dye DiSBAC to measure relative changes in V_{mem} after treatment with the drugs. All of the pharmacological treatments caused increases in fluorescence, which is indicative of depolarization. Due to inter-cell variability, however, the average increases in fluorescence after glibenclamide, monensin, and barium treatments were not statistically different from that of cells treated with a blank solution (6.95 ± 5.44 %, 5.72 ± 4.52 %, 2.17 ± 2.87 %, versus −1.65 ± 4.41 %, $p>0.05$) (Figure 1B). This variability likely arises from the inherent heterogeneity of hMSC populations [33–36], a heterogeneity that includes expression of different ionic currents [37]. In our heterogeneous population of hMSCs, we observed that for a given reagent (glibenclamide, monensin, or barium), some cells responded with V_{mem} depolarization, while other cells did not respond with any V_{mem} change. In contrast, high K^+ caused a large and significant increase in fluorescence (61.41 ± 16.70 %, $p \ll 0.001$) (Figure 1B), a response that was consistently observed in all cells. We conclude that our electrophysiological reagents do induce V_{mem} depolarization, but the heterogeneity of the cell population causes some reagents (glibenclamide, monensin, and barium) to elicit a response from only a subpopulation of cells.

3.2 Effect of electrophysiological modulation on cell content and distribution

Histological evaluation of the outer scaffolds of the bone wound model indicated that overall cell distribution and content within the scaffolds was dense and uniform. Cells filled the entire pores of the outer scaffolds regardless of treatment (Figure 2A–F). Measurement of DNA content of the scaffolds revealed that glibenclamide treatment caused a statistically significant decrease in cell content compared to monensin-treated, barium-treated, high K^+-barium-treated, and untreated scaffolds (1.5-fold, $p<0.006$; 1.5-fold, $p<0.02$; 1.5-fold, $p<0.02$; and1.6-fold, $p<0.002$) (Figure 2G). Cell distribution was less homogenous and dense in center scaffolds compared to outer scaffolds. Histological staining revealed that some scaffold pores were loosely filled with cells, other pores were only lined with cells along the pore edge, while other pores lacked cells completely (Figure 3A–F). None of the

treated center scaffolds demonstrated significant changes in DNA content compared to the untreated OS group (Figure 3G). However, among the treated scaffolds, the KB-treated group exhibited a statistically significant increase in cell content relative to both the monensin-treated and the high K^+-treated groups (1.4-fold, $p < 0.04$, and 1.6-fold, $p < 0.004$, respectively). (Figure 3G). Overall, we conclude that cell content in outer scaffolds was decreased by glibenclamide treatment compared to all conditions except high K^+ treatment, and that cell content in center scaffolds was increased by high K^+-barium treatment compared to monensin and high K+ treatments.

3.3 Effect of electrophysiological modulation on scaffold mineralization

To analyze the extent of mineralization within the bone wound model, both outer and center scaffolds were sectioned and stained with Alizarin Red, and calcium content was quantified biochemically. All outer scaffolds were positive for Alizarin Red staining (Figure 4A–F). However, staining was unevenly distributed for most scaffolds. We observed a combination of scattered punctate staining, staining of the silk pore lining, as well as broad, dense staining throughout the pores. Glibenclamide-treated outer scaffolds showed the greatest degree of uniformity, exhibiting heavy, dense staining throughout most of the scaffold (Figure 4B). Biochemical analysis of calcium content revealed that glibenclamide and monensin treatments increased calcification significantly by 2.7-fold and 1.6-fold, respectively, compared to untreated outer scaffolds ($p \ll 0.001$ and $p<0.002$, respectively) (Figure 4G). The other treatments did not have significant effects. Alizarin Red staining was greatly reduced in center scaffolds compared to outer scaffolds. We did not observe any punctate staining or any dense staining throughout entire pores. Instead, center scaffolds displayed heavy staining only along the silk pore edges (Figure 5A–H). All V_{mem} treatments altered mineral content of the center scaffolds. Only monensin treatment yielded an increase (1.8-fold) in calcium content ($p<0.03$) (Figure 5G). Glibenclamide, barium, high K^+, and high K^+/barium treatments produced significantly less calcium in the center scaffolds (4.5-fold decrease, 5.0-fold decrease, 24.2-fold decrease, and undetectable, respectively) ($p<0.04$, $p<0.03$, $p<0.007$, respectively) (Figure 5G). Thus, electrophysiological modulation of wounded bone constructs induced a response in mineralization, a late-stage osteogenic marker, and this response differed between outer and center scaffolds. Monensin increased mineralization in both outer and center scaffolds. Glibenclamide increased mineralization in outer scaffolds, but decreased mineralization in center scaffolds. Barium, high K^+, and high K^+/barium treatments had no effect on outer scaffolds, but decreased mineralization in center scaffolds.

3.4 Effect of electrophysiological treatments on expression of bone genes

We next analyzed the expression of key mRNA markers to examine transcriptional events downstream of biophysical modulation. While electrophysiology-altering reagents did not have statistically significant effects on bone transcript expression in center scaffolds, they did alter gene expression in outer scaffolds. Runx2 expression was not significantly different in treated groups compared to the untreated OS group. However, glibenclamide-treated scaffolds did show significantly lower Runx2 expression compared to barium-treated, high K^+-treated, and the high K^+/barium-treated groups (Figure 6A). Col1 expression was increased in high K^+/barium-treated groups compared to all other groups. In addition, Col1 expression in the barium-treated group was lower than in the untreated OS group (Figure 6B). ALP expression was higher in the glibenclamide-treated group compared to all groups except the monensin-treated group (Figure 6C). BSP expression was elevated in the high-K^+-treated group compared to all other groups (Figure 6D). Electrophysiological treatments therefore altered the expression of early, intermediate, and late markers of osteogenic differentiation. Each treated group exhibited a unique osteogenic gene expression profile,

suggesting that the different bioelectric treatments produced slight differences in the differentiated state of the cells.

4. Discussion

We and others have previously reported many strategies for bone tissue engineering using a wide variety of polymeric and natural biomaterials [20]. These efforts aim to stimulate important cellular events in osteochondral development and regeneration by providing appropriate biochemical and biophysical cues, with the goal of engineering implantable bone-like constructs to fill a defect. Beyond serving as implantable replacements for diseased or damaged native tissue, engineered tissues may also function as *ex vivo* platforms in which tissue response to various stimuli can be tested. Development of such pre-clinical models would be invaluable for studying the wound healing behavior of a human tissue in a tightly controlled, *ex vivo* environment.

Of particular interest in this study is the role of bioelectrical cues in regulating bone formation and healing. Clinically, electromagnetic fields have been applied to bone fractures to promote healing via direct current, capacitive coupling, or inductive coupling methods [38, 39]. However, the utility and efficacy of these treatments is still not widely accepted due to inconsistent experimental designs and variable dosages [38, 39], and the fundamental difficulty of mechanistically linking the many diverse effects of exogenous electromagnetic field exposure to changes in endogenous bioelectrical (V_{mem}) and genetic (transcriptional) cell regulatory pathways. *In vitro* studies of osteoblasts in monolayer cultures and in 3D scaffolds have shown that applied electric fields induce changes in morphology, proliferation, gene expression, differentiation markers, stress markers, and Ca^{2+} dynamics [24–27]. Less is known, however, about the role of endogenous electrical signaling, rather than exogenous electrical stimulation, in bone repair. Tissue-engineered bone offers a suitable *in vitro* model system for studying endogenous electrical properties of bone tissue during wound healing. We have previously reported an engineered 3D bone model system in which osteogenic-differentiated hMSCs are grown in porous, aqueous-derived silk fibroin scaffolds [28]. This *in vitro* model supported cell proliferation and increased several markers of the bone phenotype, including ALP activity; calcium deposition; gene expression of Col 1 and ALP; and protein expression of Col 1, osteopontin, bone sialoprotein, and matrix metalloproteinase 13 [28]. In our present study, we developed this model further to incorporate a wounding component.

In this study, we screened a number of compounds in our tissue-engineered bone wound model, specifically focusing on reagents that directly perturb resting potential [40]. One group of scaffolds was treated with monensin, an ionophore with selectivity for the Na^+ ion. Monensin-induced Na^+ currents have been shown to initiate tail regeneration following tail amputation in Xenopus laevis [41], and indeed induce the regeneration of complete Xenopus limbs [42]. We treated our engineered bone constructs with monensin to determine whether induction of a sodium current could similarly improve healing in engineered bone. Another group of scaffolds was treated with glibenclamide, an antagonist of the inward rectifying, ATP-sensitive K^+ channel (Kir 6.x). Pharmacologic modulation of Kir 6.x channel activity was previously shown to regulate osteogenic differentiation of hMSCs [29]. Additionally, expression of the various Kir6.x subunits was shown to be differentially regulated on the gene and protein level during both osteogenic and adipogenic differentiation, suggesting a possible role for Kir6.x in hMSC differentiation [43]. We used glibenclamide in our model to determine whether modulation of Kir6.x activity could stimulate osteoblast differentiation in the wound. Another group of scaffolds was treated with barium chloride, a general K^+ channel blocker, to compare the effects of specific vs. broad K^+ channel inhibition. Finally, another group of scaffolds was depolarized by high extracellular [K^+]. Modulation of V_{mem}

by high K^+ was previously shown to down-regulate the progression of hMSC differentiation [29] and also to alter the mature phenotype of differentiated cells [44]. Loss of mature phenotype could be useful for mobilizing cells in the wound environment, similar to de-differentiation events that have been reported in several systems, such as zebrafish heart and fin regeneration, urodele limb regeneration, and Schwann cell de-differentiation following nerve injury [45–48]. We included a group of scaffolds treated first with high K^+, then with barium chloride, to determine if, after responding to a de-differentiation signal, cells could also respond to another electrophysiological signal regulating differentiation.

Evaluation of cell content of the scaffolds indicated that glibenclamide-treated outer scaffolds had a significantly lower number of cells than untreated scaffolds, although this was not apparent when observing the tissue sections by eye. This indicates that hMSC-derived osteoblasts are sensitive to blockade of the ATP-sensitive Kir 6.x channel. Interestingly, however, this effect was not seen with barium chloride, a general K^+ channel blocker. Cell content is therefore decreased when Kir6.x channels specifically are antagonized. Why was there a decrease in cell numbers? Cell proliferation and differentiation are often oppositely regulated: since glibenclamide-treated outer scaffolds showed a greater amount of differentiation, there may have been a concomitant decrease in cell proliferation. Alternatively, some cells may have undergone apoptosis, another feature of bone remodeling and a part of the regeneration process [49].

After wounding, cells from our tissue-engineered bone constructs were detected in the center scaffolds. This demonstrates that the osteogenic cells do possess the potential to participate in wound healing by repopulating the wound area. This may resemble early phases of fracture healing *in vivo*, where both osteoprogenitor cells and undifferentiated mesenchymal stem cells aggregate at the wound site, then undergo proliferation and differentiation along chondrogenic and osteogenic lineages [50]. In our *in vitro* healing model, it is unclear whether the cell population in the center scaffolds arises primarily from cell migration from the surrounding scaffolds, from proliferation of a small migrating population, or from a combination of the two. Future studies may utilize lineage-tracing dyes during time-course evaluation of the wound area to follow the behavior of these cells.

The observation that even untreated cells were able to partially re-populate the wound indicates that our engineered bone model possesses a baseline degree of regenerative potential. This raises the question of how to evaluate and determine the limits to an engineered tissue's *in vitro* regenerative potential. This is analogous to defining a critical size bone defect (CSBD) in an *in vivo* wound model. Establishing such a parameter is not a trivial matter. The CSBD has been defined as the smallest sized defect that will not completely heal over the lifetime of the animal [51]. Some variants of the above CSBD definition include a defect that has less than 10% regeneration during the lifetime of the animal [52], and a segmental bone deficiency whose length is greater than 2–2.5 times the diameter of the bone [53, 54]. CSBD values can be influenced by factors including animal breed and age, bone location, surgical fixation, defect size, the presence of the periosteum, and biomechanical conditions [54, 55]. Thus, the CSBD value for an animal model is dependent both on the biology of the model and on the metric chosen to define the CSBD.

Defining an analogous CSBD value for *in vitro* studies requires further consideration of additional factors, including the ambiguity of the term 'lifetime' for an *in vitro* construct, the range of measures available for evaluating regeneration, the variability in defining when an *in vitro* wound has completely healed, and the possible irrelevancy of employing a ratiometric definition of CSBD (gap-length:bone-diameter) due to arbitrary scaffold dimensions. Because of these complications, this study did not undertake the task of defining an *in vitro* CSBD value. However, an appropriate CSBD value could be explored

using this model by investigating the effects of altering various parameters of the bone model (including dimensions of the scaffold and the wound gap) and by setting reasonable metrics with which to define complete healing and construct lifetime. In this study, rather than define an *in vitro* CSBD value, a wound gap length was chosen and the endogenous healing properties of the bone construct within the wound were characterized. Subsequently, the regenerative effect of several electrophysiological treatments was determined relative to this baseline evaluation. Because an *in vitro* model likely has lower regeneration potential compared to native tissue and because of the small size of engineered constructs used in this study (3mm in height) compared to entire bones *in vivo*, a gap-length:bone-diameter ratio was chosen that is significantly less than what has been reported for *in vivo* CSBDs (0.25 for this study vs. 2–2.5 for some CSBD criteria [53, 54]), so as not to far exceed the possibility for regeneration.

We found that the effects of electrophysiological modulation on cell differentiation within the model were not necessarily dependent on V_{mem} changes, contrary to what has been shown for osteogenic differentiation of undifferentiated hMSCs [29]. Increased mineral was observed in outer scaffolds in response to glibenclamide and monensin treatments (Figure 7A). However, glibenclamide and monensin produced neither the most nor the least change in V_{mem}: they caused slightly more depolarization than barium chloride (not statistically significant), but less depolarization compared to high K^+ treatment (statistically significant). Increased differentiation in this model is therefore not necessarily a V_{mem}-dependent response. Is it then a compound-specific effect? Glibenclamide is a blocker of the ATP-sensitive K^+ channel, while monensin is a Na^+-specific ionophore; thus, their primary actions appear to involve different ions. While it is possible that the similarity of their effects on osteogenic cells is unrelated, another possibility is that, because cell electrophysiology is dependent upon many interrelated factors, glibenclamide and monensin may have caused cells to achieve the same electrophysiological “state space” [2], and this similar state space could produce the same effect on mineralization. Testing this hypothesis will require a thorough characterization of changes in ion flux, V_{mem}, pH, and other electrophysiological parameters.

Interestingly, the effect of V_{mem} treatments differed between outer and center scaffolds in some cases, despite the fact that the outer scaffolds were the source of cells for the inner scaffolds (Figure 7A). In center scaffolds, monensin treatment stimulated a greater amount of mineralization than in untreated groups, behaving similarly in both outer and center scaffolds. Glibenclamide, high K^+, and barium treatment, however, induced a decrease in mineral not seen in outer scaffolds. A possible explanation for this difference could be that the different treatments induced a different subpopulation of cells to migrate into the wound. Intra-population heterogeneity has been well-documented in hMSCs [33, 34, 36] and is most commonly characterized in terms of the tri-lineage (osteogenic, adipogenic, chondrogenic) potential of single colony-derived strains or non-immortalized cell clones. Such work has demonstrated that hMSC clones differ from one other with respect to their differentiation potential [33, 34, 36], and that specific MSC functions are restricted to distinct subpopulations [56]. If hMSC heterogeneity is the underlying factor for the observations in the present study, the monensin-responding migratory cells could be more differentiated than the migratory cells responding to the other compounds (Figure 7B), and this subpopulation could be responsible for the observed increased mineral in the center scaffolds. Future work characterizing the stem-related, osteogenic-related, and electrophysiology-related properties of these different cell populations could provide valuable insight into the identities of cells participating in wound healing and how to design therapies to target specific populations.

An alternate hypothesis is that the initial migratory cells may differ not in their differentiated state, but in their electrophysiological state (Figure 7C). These initial differences in electrophysiology may then cause the population in the center scaffolds to respond differently to the treatment compounds, resulting in a subsequent effect on differentiation. Heterogeneity in cell electrophysiology has been reported in other cell populations such as neuroblastoma cells and has even been shown to contribute to differences in the differentiation capacities and lineage biases of cell subpopulations [57]. This hypothesis also implies that electrophysiological differences may be related to both cell migratory and differentiation capacities; indeed, a connection between electrophysiology and cell migration [4] or differentiation [3] has been demonstrated previously. As with the hypothesis of an electrophysiological state space that governs cell behavior, further study would require a comprehensive characterization of various bioelectric parameters to identify the differences between cell populations and whether these differences are functionally relevant for cell migration and differentiation. Additionally, to elucidate whether heterogeneity (either cellular or electrophysiological) is truly responsible for the observed differential effects, similar *in vitro* wound healing experiments can be conducted to see whether the same behavior is observed when a clonally-identical pre-osteoblastic cell line is used instead of primary cells.

Another potential explanation for the different mineralization responses could be the differences in the microenvironment of the wound area compared to that of the surrounding tissue. When wound-infiltrating cells first encounter the center scaffold (the wound area), they experience a completely different biochemical and biomechanical landscape compared to the osteogenic environment of the bulk tissue. Because the wound is initially devoid of cells, there is likely decreased paracrine signaling due to the lack of cytokine and growth factor secretion by nearby osteoblasts. The cells also likely experience different interactions with their substrate: instead of interacting with osteoblast-secreted extracellular matrix (ECM), the cells first encounter silk only as their substrate. The mechanical properties of the wound may also differ from the non-wounded area because of the lack of mineral. Additionally, the act of wounding the construct may induce the release of some injury-responsive factors in a spatial gradient [58], where cells local to the injury site experience the greatest concentrations of these factors. A combination of these factors likely contributes to a distinct wound-specific microenvironment that may alter the osteogenic behavior of cells in the wound vicinity. The hypothesis that different biochemical and biomechanical factors can alter cell responses to electrophysiological compounds implies that chemical and mechanical signaling underlie the bioelectric response, and indeed, these mechanisms have been proposed and explored [2, 5, 59].

5. Conclusion

We present a model of *in vitro* wound healing in tissue-engineered bone as a platform in which tissue electrophysiology may be rationally modulated to stimulate regeneration. Using this model, we screened several bioelectric modulators and identified two pharmacological agents that augmented cell differentiation but had distinct effects on cell behavior in the wound area versus in the surrounding tissue. These data suggest that further investigation of the observed healing responses may take several interesting directions, including evaluating the heterogeneity of the osteogenic and electrophysiological properties of the osteoblast population, profiling the secretion of different soluble factors and ECM by cells in the wound versus the surrounding tissue, and quantifying the differences in mechanical properties due to the different ECM composition in the wound versus the surrounding tissue. Such a comprehensive model would integrate cellular, biochemical, biomechanical, and electrophysiological data into an *in vitro* platform that would not only allow screening of

potential therapeutically useful compounds, but also provide insight into how bioelectrical signaling is integrated in the global wound healing picture.

Acknowledgments

We would like to thank Reynald Lescarbeau, Rebecca Scholl Hayden, Julia Yelick, and Anne Strobelt for their help with silk scaffold preparation, tissue culture, and scaffold analyses in preliminary bone healing experiments. S.S. thanks the NSF for funding through the Graduate Research Fellowship Program. We also thank the NIH for support through the Tissue Engineering Resource Center (P41 EB002520), R01 AR005593, and R01 AR061988.

References

1. Blackiston DJ, McLaughlin KA, Levin M. Bioelectric controls of cell proliferation: ion channels, membrane voltage, and the cell cycle. Cell Cycle. 2009; 8(21):3527–3536.
2. Levin M, Stevenson CG. Regulation of cell behavior and tissue patterning by bioelectrical signals: challenges and opportunities for biomedical engineering. Annu Rev Biomed Eng. 2012; 14:295–323. [PubMed: 22809139]
3. Sundelacruz S, Levin M, Kaplan DL. Role of membrane potential in the regulation of cell proliferation and differentiation. Stem Cell Rev. 2009; 5(3):231–246. [PubMed: 19562527]
4. Zhao M. Electrical fields in wound healing - An overriding signal that directs cell migration. Semin Cell Dev Biol. 2009; 20(6):674–682. [PubMed: 19146969]
5. Levin M. Large-scale biophysics: ion flows and regeneration. Trends Cell Biol. 2007; 17(6):261–270. [PubMed: 17498955]
6. Borgens RB. Endogenous ionic currents traverse intact and damaged bone. Science. 1984; 225(4661):478–482. [PubMed: 6740320]
7. Borgens RB, Vanable JW Jr, Jaffe LF. Bioelectricity and regeneration: Large currents leave the stumps of regenerating newt limbs. Proc Natl Acad Sci U S A. 1977; 74(10):4528–4532. [PubMed: 270701]
8. Chiang M, Robinson KR, Vanable JW Jr. Electrical fields in the vicinity of epithelial wounds in the isolated bovine eye. Exp Eye Res. 1992; 54(6):999–1003. [PubMed: 1521590]
9. Foulds IS, Barker AT. Human skin battery potentials and their possible role in wound healing. Br J Dermatol. 1983; 109(5):515–522. [PubMed: 6639877]
10. Borgens RB, Vanable JW Jr, Jaffe LF. Role of subdermal current shunts in the failure of frogs to regenerate. J Exp Zool. 1979; 209(1):49–56. [PubMed: 314968]
11. Jenkins LS, Duerstock BS, Borgens RB. Reduction of the current of injury leaving the amputation inhibits limb regeneration in the red spotted newt. Dev Biol. 1996; 178(2):251–262. [PubMed: 8812127]
12. Borgens RB, Vanable JW Jr, Jaffe LF. Bioelectricity and regeneration: Initiating of frog limb regeneration by minute currents. J Exp Zool. 1977; 200:403–416. [PubMed: 301554]
13. Sisken BF, Fowler I. Induction of limb regeneration in the chick-embryo. Anat Rec. 1981; 199(3):A238–A239.
14. Smith SD. Induction of partial limb regeneration in Rana pipiens by galvanic stimulation. Anat Rec. 1967; 158:89–97. [PubMed: 6033441]
15. Zhao M, Song B, Pu J, Wada T, Reid B, Tai G, et al. Electrical signals control wound healing through phosphatidylinositol-3-OH kinase-gamma and PTEN. Nature. 2006; 442(7101):457–460. [PubMed: 16871217]
16. Zhao Z, Watt C, Karystinou A, Roelofs AJ, McCaig CD, Gibson IR, et al. Directed migration of human bone marrow mesenchymal stem cells in a physiological direct current electric field. Eur Cell Mater. 2011; 22:344–358. [PubMed: 22125259]
17. Song B, Zhao M, Forrester J, McCaig C. Nerve regeneration and wound healing are stimulated and directed by an endogenous electrical field in vivo. J Cell Sci. 2004; 117(20):4681–4690. [PubMed: 15371524]

18. Zhao M, Bai H, Wang E, Forrester JV, McCaig CD. Electrical stimulation directly induces preangiogenic responses in vascular endothelial cells by signaling through VEGF receptors. J Cell Sci. 2004; 117(3):397–405. [PubMed: 14679307]
19. Hannouche D, Petite H, Sedel L. Current trends in the enhancement of fracture healing. J Bone Joint Surg Br. 2001; 83(2):157–164. [PubMed: 11284556]
20. Sundelacruz S, Kaplan DL. Stem cell- and scaffold-based tissue engineering approaches to osteochondral regenerative medicine. Semin Cell Dev Biol. 2009; 20(6):646–655. [PubMed: 19508851]
21. Mills LA, Simpson AHRW. In vivo models of bone repair. J Bone Joint Surg Br. 2012; 94 B(7): 865–874. [PubMed: 22733938]
22. Schindeler A, McDonald MM, Bokko P, Little DG. Bone remodeling during fracture repair: The cellular picture. Semin Cell Dev Biol. 2008; 19(5):459–466. [PubMed: 18692584]
23. Auer JA, Goodship A, Arnoczky S, Pearce S, Price J, Claes L, et al. Refining animal models in fracture research: Seeking consensus in optimising both animal welfare and scientific validity for appropriate biomedical use. BMC Musculoskelet Disord. 2007; 8(72)
24. Hess R, Jaeschke A, Neubert H, Hintze V, Moeller S, Schnabelrauch M, et al. Synergistic effect of defined artificial extracellular matrices and pulsed electric fields on osteogenic differentiation of human MSCs. Biomaterials. 2012; 33(35):8975–8985. [PubMed: 22995709]
25. Hronik-Tupaj M, Rice WL, Cronin-Golomb M, Kaplan DL, Georgakoudi I. Osteoblastic differentiation and stress response of human mesenchymal stem cells exposed to alternating current electric fields. Biomed Eng Online. 2011; 10(9)
26. Icaro Cornaglia A, Casasco M, Riva F, Farina A, Fassina L, Visai L, et al. Stimulation of osteoblast growth by an electromagnetic field in a model of bone-like construct. Eur J Histochem. 2006; 50(3):199–203. [PubMed: 16920643]
27. Tsai MT, Li WJ, Tuan RS, Chang WH. Modulation of osteogenesis in human mesenchymal stem cells by specific pulsed electromagnetic field stimulation. J Orthop Res. 2009; 27(9):1169–1174. [PubMed: 19274753]
28. Kim HJ, Kim UJ, Vunjak-Novakovic G, Min BH, Kaplan DL. Influence of macroporous protein scaffolds on bone tissue engineering from bone marrow stem cells. Biomaterials. 2005; 26(21): 4442–4452. [PubMed: 15701373]
29. Sundelacruz S, Levin M, Kaplan DL. Membrane potential controls adipogenic and osteogenic differentiation of mesenchymal stem cells. PLoS ONE. 2008; 3(11):e3737. [PubMed: 19011685]
30. Dominici M, Le Blanc K, Mueller I, Slaper-Cortenbach I, Marini F, Krause D, et al. Minimal criteria for defining multipotent mesenchymal stromal cells. The International Society for Cellular Therapy position statement. Cytotherapy. 2006; 8(4):315–317. [PubMed: 16923606]
31. Meinel L, Fajardo R, Hofmann S, Langer R, Chen J, Snyder B, et al. Silk implants for the healing of critical size bone defects. Bone. 2005; 37(5):688–698. [PubMed: 16140599]
32. Adams DS, Levin M. General principles for measuring resting membrane potential and ion concentration using fluorescent bioelectricity reporters. Cold Spring Harb Protoc. 2012; 7(4):385–397. [PubMed: 22474653]
33. Kuznetsov SA, Krebsbach PH, Satomura K, Kerr J, Riminucci M, Benayahu D, et al. Single-colony derived strains of human marrow stromal fibroblasts form bone after transplantation in vivo. J Bone Miner Res. 1997; 12(9):1335–1347. [PubMed: 9286749]
34. Muraglia A, Cancedda R, Quarto R. Clonal mesenchymal progenitors from human bone marrow differentiate in vitro according to a hierarchical model. J Cell Sci. 2000; 113(7):1161–1166. [PubMed: 10704367]
35. Phinney DG, Kopen G, Righter W, Webster S, Tremain N, Prockop DJ. Donor variation in the growth properties and osteogenic potential of human marrow stromal cells. J Cell Biochem. 1999; 75(3):424–436. [PubMed: 10536366]
36. Russell KC, Phinney DG, Lacey MR, Barrilleaux BL, Meyertholen KE, O'Connor KC. In vitro highcapacity assay to quantify the clonal heterogeneity in trilineage potential of mesenchymal stem cells reveals a complex hierarchy of lineage commitment. Stem Cells. 2010; 28(4):788–798. [PubMed: 20127798]

37. Heubach JF, Graf EM, Leutheuser J, Bock M, Balana B, Zahanich I, et al. Electrophysiological properties of human mesenchymal stem cells. J Physiol. 2004; 554(3):659–672. [PubMed: 14578475]
38. Aaron RK, Ciombor DM, Simon BJ. Treatment of nonunions with electric and electromagnetic fields. Clin Orthop Relat Res. 2004; (419):21–29. [PubMed: 15021127]
39. Isaacson BM, Bloebaum RD. Bone bioelectricity: What have we learned in the past 160 years? J Biomed Mater Res A. 2010; 95(4):1270–1279. [PubMed: 20878899]
40. Adams DS, Levin M. Endogenous voltage gradients as mediators of cell-cell communication: strategies for investigating bioelectrical signals during pattern formation. Cell Tissue Res. 2012:1–12.
41. Tseng AS, Beane WS, Lemire JM, Masi A, Levin M. Induction of vertebrate regeneration by a transient sodium current. J Neurosci. 2010; 30(39):13192–13200. [PubMed: 20881138]
42. Tseng A, Levin M. Cracking the bioelectric code: Probing endogenous ionic controls of pattern formation. Commun Integr Biol. 2013; 6(1):e22595. [PubMed: 23802040]
43. Diehlmann A, Bork S, Saffrich R, Veh RW, Wagner W, Derst C. KATP channels in mesenchymal stromal stem cells: Strong up-regulation of Kir6. 2 subunits upon osteogenic differentiation. Tissue Cell. 2011; 43(5):331–336. [PubMed: 21820692]
44. Sundelacruz S, Levin M, Kaplan DL. Depolarization alters phenotype, maintains plasticity of predifferentiated mesenchymal stem cells. Tissue Eng. 2013 in press.
45. Jopling C, Sleep E, Raya M, Marti M, Raya A, Izpisua Belmonte JC. Zebrafish heart regeneration occurs by cardiomyocyte dedifferentiation and proliferation. Nature. 2010; 464(7288):606–609. [PubMed: 20336145]
46. Knopf F, Hammond C, Chekuru A, Kurth T, Hans S, Weber CW, et al. Bone regenerates via dedifferentiation of osteoblasts in the zebrafish fin. Dev Cell. 2011; 20(5):713–724. [PubMed: 21571227]
47. Kragl M, Knapp D, Nacu E, Khattak S, Maden M, Epperlein HH, et al. Cells keep a memory of their tissue origin during axolotl limb regeneration. Nature. 2009; 460(7251):60–65. [PubMed: 19571878]
48. Mirsky R, Woodhoo A, Parkinson DB, Arthur-Farraj P, Bhaskaran A, Jessen KR. Novel signals controlling embryonic Schwann cell development, myelination and dedifferentiation. J Peripher Nerv Syst. 2008; 13(2):122–135. [PubMed: 18601657]
49. Hock JM, Krishnan V, Onyia JE, Bidwell JP, Milas J, Stanislaus D. Osteoblast apoptosis and bone turnover. J Bone Miner Res. 2001; 16(6):975–984. [PubMed: 11393794]
50. Kraus KH, Kirker-Head C. Mesenchymal stem cells and bone regeneration. Vet Surg. 2006; 35(3): 232–242. [PubMed: 16635002]
51. Schmitz JP, Hollinger JO. The critical size defect as an experimental model for craniomandibulofacial nonunions. Clin Orthop Relat Res. 1986; 205:299–308. [PubMed: 3084153]
52. Gugala Z, Gogolewski S. Regeneration of segmental diaphyseal defects in sheep tibiae using resorbable polymeric membranes: A preliminary study. J Orthop Trauma. 1999; 13(3):187–195. [PubMed: 10206250]
53. Gugala Z, Lindsey RW, Gogolewski S. New approaches in the treatment of critical-size segmental defects in long bones. Macromol Symp. 2007; 253:147–161.
54. Lindsey RW, Gugala Z, Milne E, Sun M, Gannon FH, Latta LL. The efficacy of cylindrical titanium mesh cage for the reconstruction of a critical-size canine segmental femoral diaphyseal defect. J Orthop Res. 2006; 24(7):1438–1453. [PubMed: 16732617]
55. Rimondini L, Nicoli-Aldini N, Fini M, Guzzardella G, Tschon M, Giardino R. In vivo experimental study on bone regeneration in critical bone defects using an injectable biodegradable PLA/PGA copolymer. Oral Surg Oral Med Oral Pathol Oral Radiol Endod. 2005; 99(2):148–154. [PubMed: 15660083]
56. Phinney DG. Functional heterogeneity of mesenchymal stem cells: Implications for cell therapy. J Cell Biochem. 2012; 113(9):2806–2812. [PubMed: 22511358]

57. Biagiotti T, D'Amico M, Marzi I, Di Gennaro P, Arcangeli A, Wanke E, et al. Cell renewing in neuroblastoma: Electrophysiological and immunocytochemical characterization of stem cells and derivatives. Stem Cells. 2006; 24(2):443–453. [PubMed: 16100002]

58. Niethammer P, Grabher C, Look AT, Mitchison TJ. A tissue-scale gradient of hydrogen peroxide mediates rapid wound detection in zebrafish. Nature. 2009; 459(7249):996–999. [PubMed: 19494811]

59. Hart FX. Integrins may serve as mechanical transducers for low-frequency electric fields. Bioelectromagnetics. 2006; 27(6):505–508. [PubMed: 16715526]

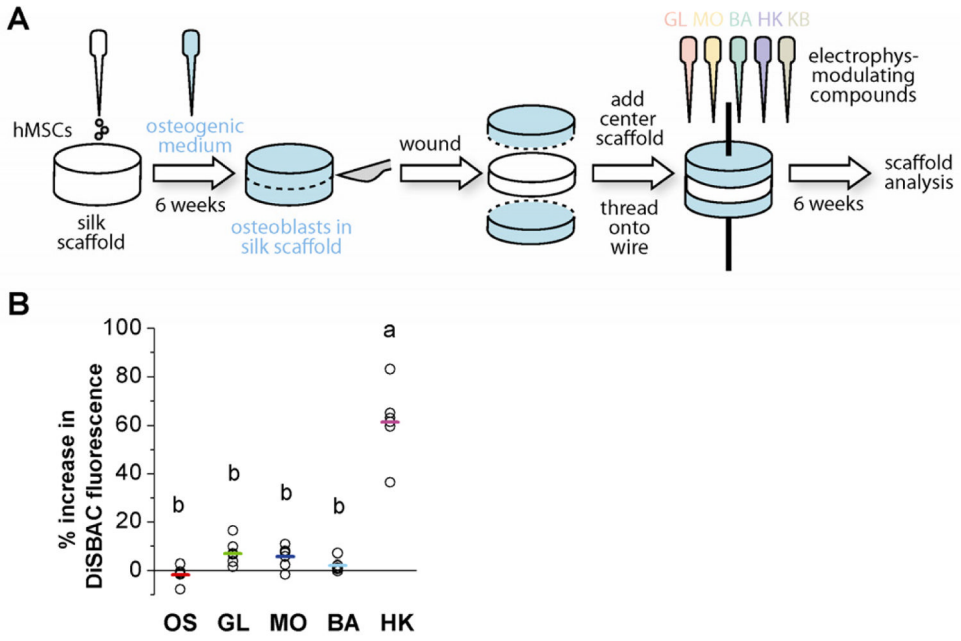

Figure 1. Schematic representation of wound model (A) and V_{mem} changes induced by bioelectric treatments (B)

(A) Undifferentiated human mesenchymal stem cells (hMSCs) were seeded onto silk sponges with pore sizes of 500–600 μm in diameter. Cells were differentiated toward the osteoblastic lineage for six weeks. At Week 6, scaffolds were cut in half in cross-section. A fresh, acellular silk scaffold was inserted between the cut halves, and the layered structure was threaded onto a stainless steel wire. The tissues were cultured for an additional six weeks with or without electrophysiology-modulating compounds: glibenclamide (GL, 10 μM), monensin (MO, 10 nM), barium chloride (BA, 100 μM), high K^+ (HK, 40 mM), or a sequential treatment of HK and BA (KB, 3 weeks HK, 3 weeks BA). At the end of twelve weeks, scaffolds were collected for analyses and compared to untreated osteogenic (OS) scaffolds. (B) HMSC-derived osteoblasts were stained with voltage-sensitive, fluorescent dye DiSBAC and imaged before and after treatment with electrophysiology-modulating compounds. Fluorescence intensity was quantified and is displayed as % change from pre-treatment values, with a positive value indicating V_{mem} depolarization. Each data point (open circle) represents the % change calculated per field of view. The average % change over multiple fields of view is indicated with a colored bar for each treatment. A one-way ANOVA test was performed, followed by the Tukey-Kramer post-hoc test. Groups that are not significantly different ($p > 0.05$) are labeled with the same letter.

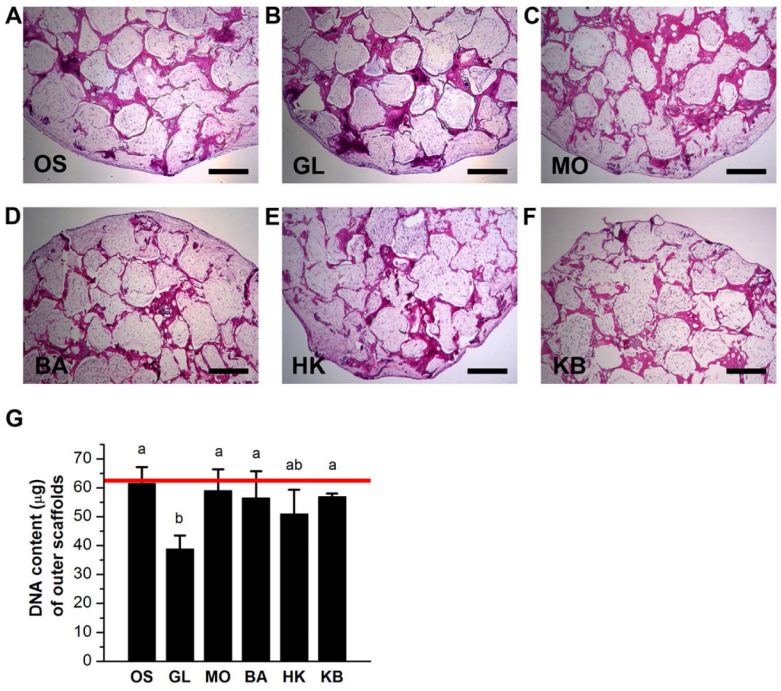

Figure 2. Cell content and distribution within outer scaffolds of wound model

(A–F) Hematoxylin and eosin staining of outer scaffolds after twelve weeks of culture. At Week 6, scaffolds were treated with: glibenclamide (GL, 10 μM), monensin (MO, 10 nM), barium chloride (BA, 100 μM), high K^+ (HK, 40 mM), or a sequential treatment of HK and BA (KB, 3 weeks HK, 3 weeks BA), or were left untreated (OS). Scale bar = 500 μm. (G) Quantification of DNA content of the outer scaffolds. Data points in bar graph are mean μg DNA ± standard deviation. A one-way ANOVA test was performed, followed by the Tukey-Kramer post-hoc test. Groups that are not significantly different ($p > 0.05$) are labeled with the same letter. Red line: DNA content of pre-cultured scaffold at Week 6 (mean μg DNA) prior to wounding.

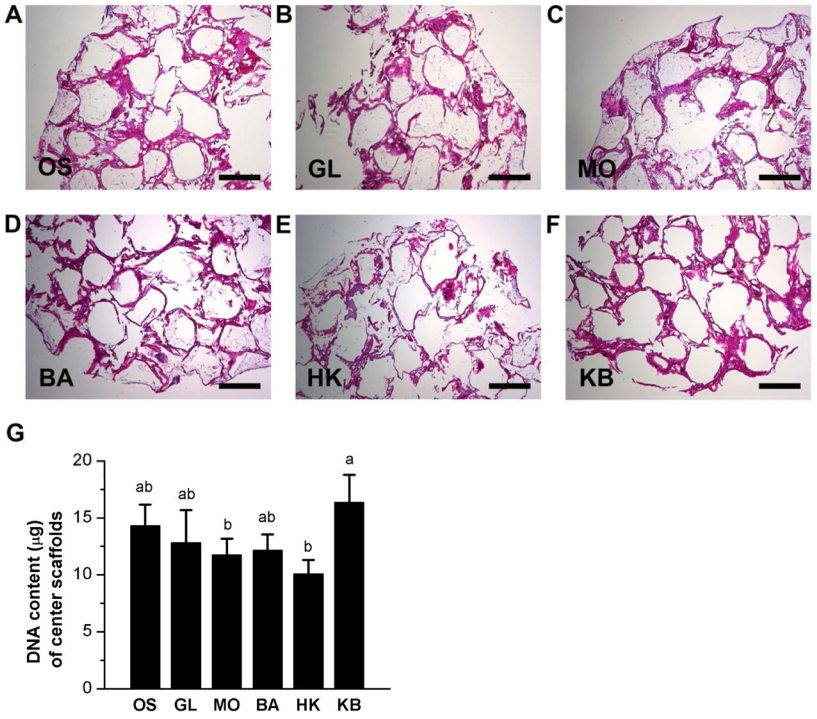

Figure 3. Cell content and distribution within center scaffolds of wound model

(A–F) Hematoxylin and eosin staining of center scaffolds after twelve weeks of culture. At Week 6, scaffolds were treated with: glibenclamide (GL, 10 μM), monensin (MO, 10 nM), barium chloride (BA, 100 μM), high K^+ (HK, 40 mM), or a sequential treatment of HK and BA (KB, 3 weeks HK, 3 weeks BA), or were left untreated (OS). Scale bar = 500 μm. (G) Quantification of DNA content of the center scaffolds. Data points are mean μg DNA ± standard deviation. A one-way ANOVA test was performed, followed by the Tukey-Kramer post-hoc test. Groups that are not significantly different ($p > 0.05$) are labeled with the same letter.

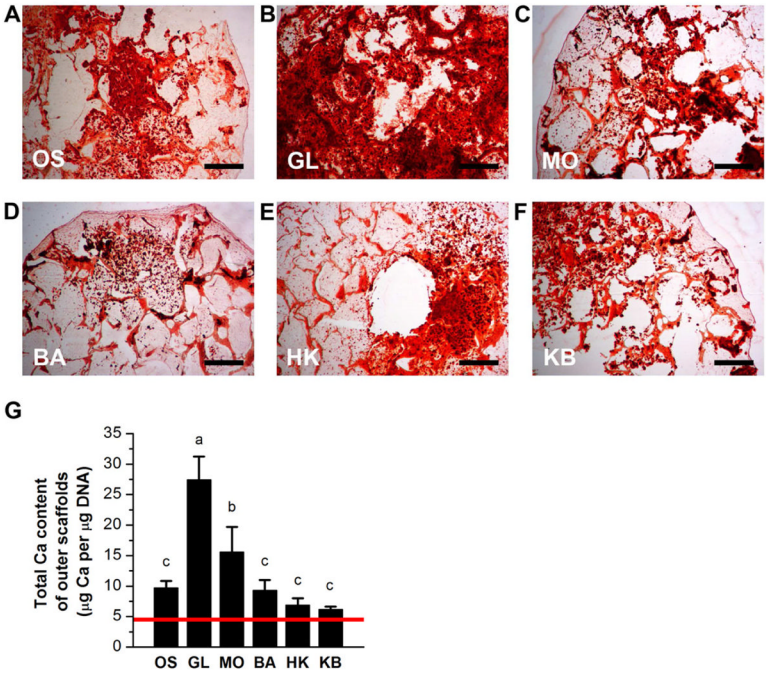

Figure 4. Mineralization of outer scaffolds of wound model

(A–F) Alizarin Red S staining of outer scaffolds after twelve weeks of culture. At Week 6, scaffolds were treated with: glibenclamide (GL, 10 μM), monensin (MO, 10 nM), barium chloride (BA, 100 μM), high K^+ (HK, 40 mM), or a sequential treatment of HK and BA (KB, 3 weeks HK, 3 weeks BA), or were left untreated (OS). Scale bar = 500 μm. (G) Quantification of calcium content of the outer scaffolds. Data points in bar graph are mean calcium content normalized to DNA content (μg Ca per μg DNA) ± standard deviation. A one-way ANOVA test was performed, followed by the Tukey-Kramer post-hoc test. Groups that are not significantly different ($p > 0.05$) are labeled with the same letter. Red line: Mean normalized calcium content of pre-cultured scaffold at Week 6 (μg Ca per μg DNA) prior to wounding.

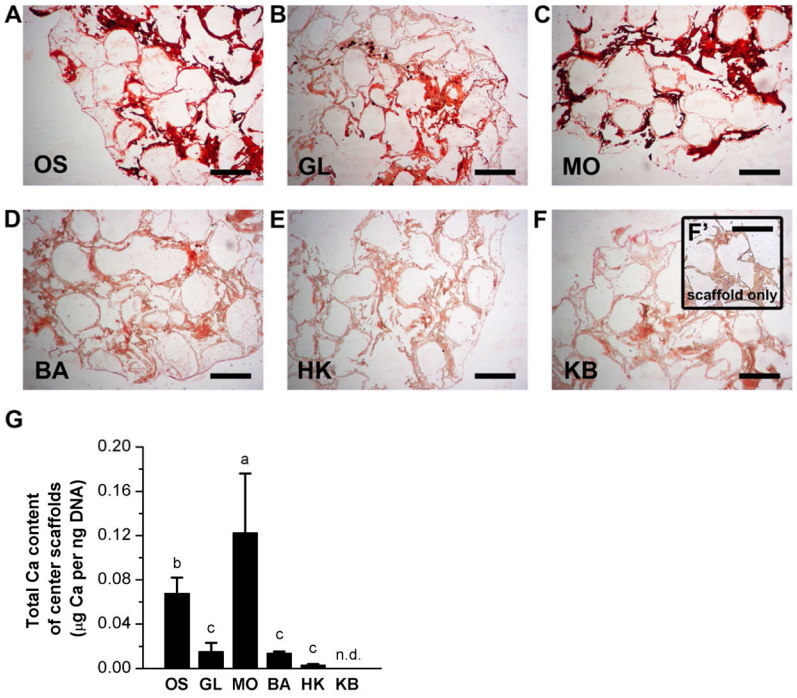

Figure 5. Mineralization of center scaffolds of wound model

(A–F) Alizarin Red S staining of center scaffolds after twelve weeks of culture. At Week 6, scaffolds were treated with: glibenclamide (GL, 10 μM), monensin (MO, 10 nM), barium chloride (BA, 100 μM), high K^+ (HK, 40 mM), or a sequential treatment of HK and BA (KB, 3 weeks HK, 3 weeks BA), or were left untreated (OS). (F') Alizarin Red S staining of unseeded silk scaffold (negative control). Scale bar = 500 μm. (G) Quantification of calcium content of the center scaffolds. Data points are mean calcium content normalized to DNA content (μg Ca per μg DNA) ± standard deviation. A one-way ANOVA test was performed, followed by the Tukey-Kramer post-hoc test. Groups that are not significantly different ($p > 0.05$) are labeled with the same letter. N.d., not detected.

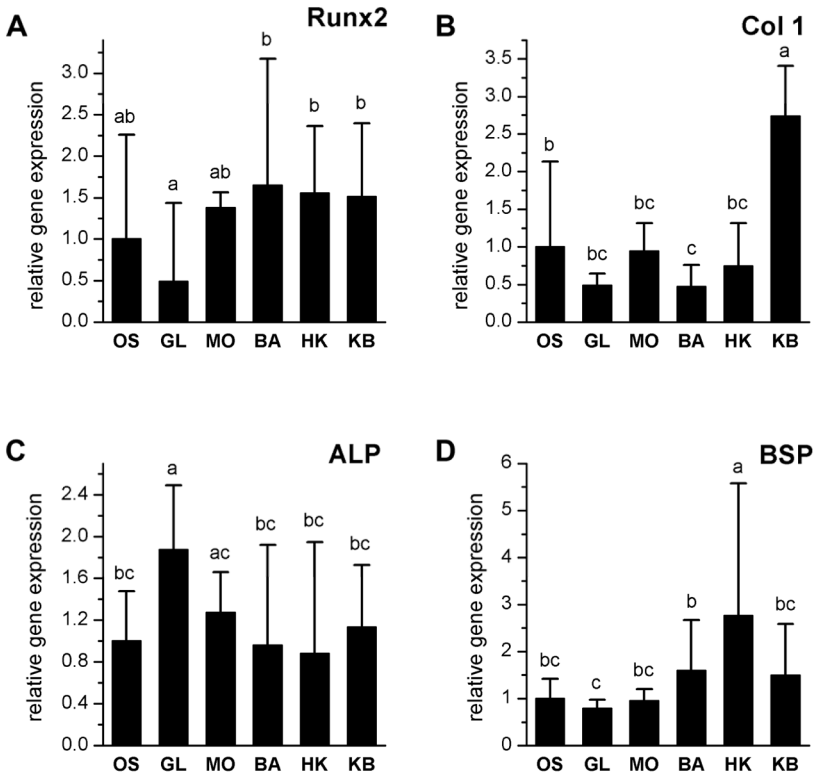

Figure 6. Expression of osteogenic genes in osteoblasts in outer scaffolds

Expression of runt-related transcription factor 2 (Runx2), collagen I alpha 1 (Col 1), alkaline phosphatase (ALP), and bone sialoprotein (BSP) was quantified by real time RT-PCR in outer scaffolds treated with glibenclamide (GL, 10 μM), monensin (MO, 10 nM), barium chloride (BA, 100 μM), high K^+ (HK, 40 mM), or a sequential treatment of HK and BA (KB, 3 weeks HK, 3 weeks BA). Results were normalized to the housekeeping gene GAPDH and were plotted as fold-change relative to untreated scaffolds (OS). Data points are relative expression (A.U.) ± standard deviation. A one-way ANOVA test was performed, followed by the Tukey-Kramer post-hoc test. Groups that are not significantly different ($p > 0.05$) are labeled with the same letter.

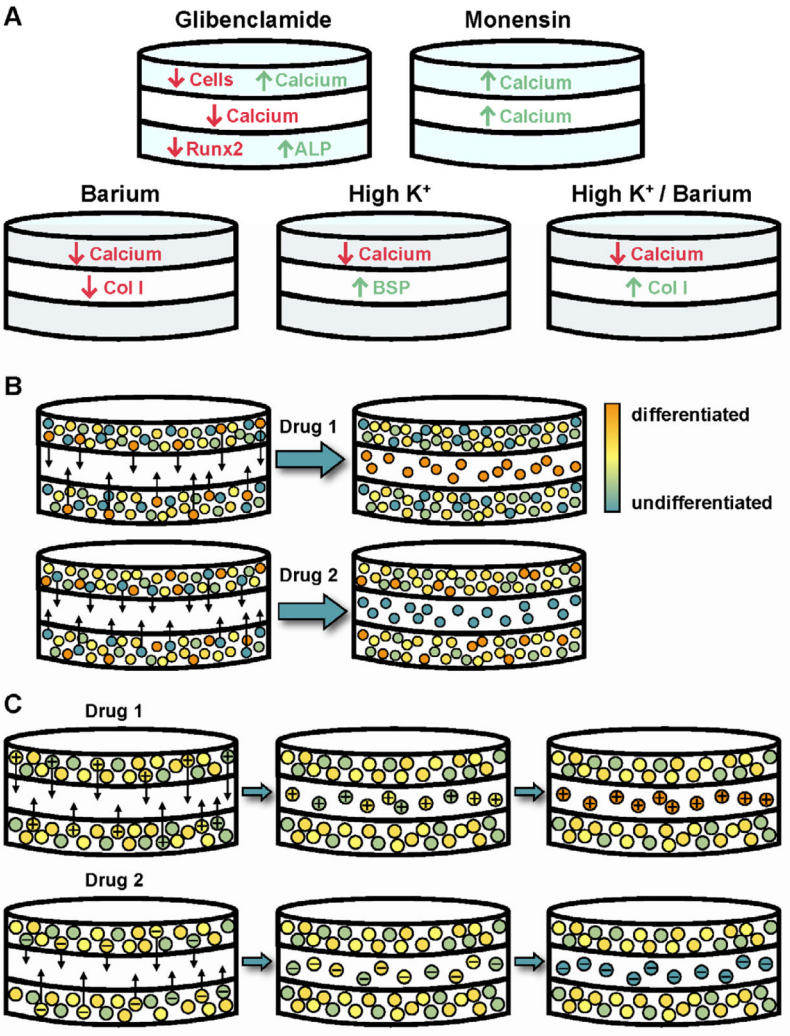

Figure 7. Electrophysiological modulation of osteogenic scaffolds: summary of cell responses and proposed models

(A) Schematic summarizing the effects of glibenclamide, monensin, barium, high K^+, and high K^+/barium on cell content, mineralization, and gene expression in outer and center scaffolds. (B) Model of cell response to electrophysiological modulation: Outer scaffolds contain a heterogeneous mixture of cells at various stages of differentiation. Each electrophysiological reagent mobilizes a specific subpopulation of cells (at a particular differentiated state, depicted in the figure by different colors) to migrate into the wound center, resulting in differences in differentiation level between outer and center scaffolds, as well as between treated groups. (C) Alternate model of cell response to electrophysiological modulation: Migratory cells are determined not by differentiated status, but by electrophysiological state. Each reagent targets a subpopulation of cells that is in a particular bioelectric state (depicted in the figure by a '+' or '−'). This targeted subpopulation migrates into the center scaffold, where it then continues to respond to the reagent by up- or down-regulating differentiation.